4π-Periodic Supercurrent from Surface States in Cd_3As_2 Nanowire-Based Josephson Junctions

An-Qi Wang,[1,2,*] Cai-Zhen Li,[2,6,*] Chuan Li,[3,*] Zhi-Min Liao,[2,4,5,†] Alexander Brinkman,[3,‡] and Da-Peng Yu[6]
[1]*Academy for Advanced Interdisciplinary Studies, Peking University, Beijing 100871, China*
[2]*State Key Laboratory for Mesoscopic Physics, School of Physics, Peking University, Beijing 100871, China*
[3]*MESA+ Institute for Nanotechnology, University of Twente, 7500 AE Enschede, Netherlands*
[4]*Beijing Key Laboratory of Quantum Devices, Peking University, Beijing 100871, China*
[5]*Collaborative Innovation Center of Quantum Matter, Beijing 100871, China*
[6]*Shenzhen Institute for Quantum Science and Engineering and Department of Physics, Southern University of Science and Technology, Shenzhen 518055, China*

(Received 19 June 2018; published 7 December 2018)

The combination of superconductivity and surface states in Dirac semimetal can produce a 4π-periodic supercurrent in a Josephson junction configuration, which can be revealed by the missing of odd Shapiro steps (especially the $n = 1$ step). However, the suppression of the $n = 1$ step is also anticipated in the high-power oscillatory regime of the ordinary 2π-periodic Josephson effect, which is irrelevant to the 4π-periodic supercurrent. Here, in order to identify the origin of the suppressed $n = 1$ step, we perform the measurements of radio frequency irradiation on Nb–Dirac semimetal Cd_3As_2 nanowire–Nb junctions with continuous power dependence at various frequencies. Besides the $n = 1$ step suppression, we uncover a residual supercurrent of first node at the $n = 0$ step, which provides a direct and predominant signature of the 4π-periodic supercurrent. Furthermore, by tuning the gate voltage, we can modulate the surface and bulk state contribution and the visibility of the $n = 1$ step. Our results provide deep insights to explore the topological superconductivity in Dirac semimetals.

DOI: 10.1103/PhysRevLett.121.237701

The topological surface state is predicted to host topological superconductivity when it is coupled to s-wave superconductors [1]. Proximity-effect-induced unconventional superconductivity in topological insulators has been reported, e.g., Josephson supercurrent through the surface state [2,3], zero bias conductance peak in the vortex center [4,5], and missing odd Shapiro steps under radio frequency (rf) irradiation [6,7]. With nontrivial Fermi-arc surface states [8–11], Dirac semimetals have also been predicted to possess both intrinsic and extrinsic (proximity effect-induced) topological superconductivity [12–15].Cd_3As_2, as a stable 3D Dirac semimetal, has been identified to have unique bulk Dirac cones and nontrivial topological surface states [14, 16–18]. Many exotic transport properties, such as ultrahigh carrier mobility [19], chiral anomaly induced negative magnetoresistance [20], the π-Aharonov-Bohm (A-B) effect [21,22], and Weyl orbit related quantum oscillations [23,24], have been demonstrated in Cd_3As_2. Unconventional superconductivity has also been observed in Cd_3As_2 through specific experiments, including the point-contact technique, high-pressure condition, etc. [25–27].

Similar to the topological insulators, helical surface states in Cd_3As_2 can also give rise to topologically protected gapless Andreev bound states through an s-wave Josephson link [28–31], which produce 4π-periodic supercurrent [6,7,32]. In the static case, 4π-periodic supercurrent tends to restore 2π periodicity, as a result of various relaxation processes [33,34]. The response in the gigahertz regime, namely, the Shapiro steps, can provide sufficient information within the lifetime of 4π- periodic modes [32]. For a pure 4π-periodic supercurrent, only even Shapiro steps should be present. Experimentally, the suppression of the $n = 1$ step is usually more significant than other odd steps, probably due to the finite capacitive effect or Joule overheating [35,36]. Recently, missing of the $n = 1$ Shapiro step has been observed in exfoliated Cd_3As_2 at low frequency irradiation [37]. However, it is still difficult to distinguish the 4π-periodic supercurrent because the missing of the $n = 1$ step can also be observed in the high-power oscillatory regime of the conventional 2π Josephson effect [6]. Moreover, for Dirac semimetals, the bulk conduction is inevitable, and, therefore, the 2π-periodic contribution should always exist and the 4π-periodic supercurrent cannot make the odd steps completely disappear. Consequently, tunable surface and bulk state contribution and power-dependent measurements are highly desirable to reveal the 4π-periodic supercurrent.

Here we employ Cd_3As_2 nanowire to reveal the surface-related 4π-periodic supercurrent, taking advantage of its large surface-to-volume ratio and easy gate modulation. The irradiation frequency, rf power, and gate dependence of the Shapiro steps in Nb $-$ Cd_3As_2 nanowire–Nb Josephson

junctions are systematically investigated. Besides the $n = 1$ step suppression, we observe residual supercurrent at the $n = 0$ step, which provides a direct signature of 4π-periodic contribution. For deep insight of this 4π-periodic supercurrent, we study the gate dependence of the rf results. By tuning the gate voltage to enhance the surface state contribution, the odd ($n = 1$) Shapiro step is further suppressed, stabilizing its surface origin of the 4π-periodic supercurrent.

The Cd_3As_2 nanowires were synthesized via the chemical vapor deposition method, which are of high-crystal quality [20]. The nanowire has large surface-to-volume ratio and demonstrates abundant surface-related transport properties [21,22]. Synthesized Cd_3As_2 nanowires were then transferred on silicon substrate with 285 nm-thick SiO_2 layer, which serves as a back gate to modulate the carrier density. The selected nanowire diameter is ~90 nm. After an Ar etching process to remove the oxidized layer, Nb/Pd contacts were deposited by magnetron sputtering. A schematic of the Josephson junction is displayed in Fig. 1(a). Several junctions of different channel lengths were fabricated and investigated, revealing the surface states carried supercurrent [38]. In this work, we mainly focus on the unconventional rf response of the surface state transport. The length of the junction presented here is $L \sim 400$ nm. Electrical transport measurements were carried out in a dilution refrigerator with a base temperature of 12 mK. In rf measurements, the involved Josephson junction was irradiated via a coaxial line, in which an rf-driving current was coupled with dc current bias I_{dc} together to induce phase-locked Shapiro steps.

Figure 1(b) presents the mapping of differential resistance dV/dI as a function of I_{dc} and gate voltage V_g, where the I_{dc} is swept from negative to positive. The upper boundary of the dark blue region indicates the critical current I_c, corresponding to V_g sweeping. When varying V_g from 10 to −20 V, the critical current I_c decreases first and tends to saturate afterwards on the whole. The small I_c in the hole region is due to the much lower hole mobility

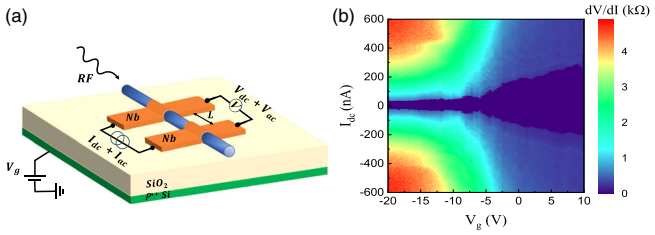

FIG. 1. Observation of supercurrent in Nb-Cd_3As_2 nanowire-Nb junction. (a) Schematic of the measurement setup. rf radiation is applied to the device through a coaxial line. The junction length $L = 400$ nm. (b) Map of differential resistance dV/dI as a function of dc current bias I_{dc} for various gate voltages. The upper boundary of the dark blue region indicates the critical current I_c, varying with V_g sweeping.

and the supercurrent from the bulk state may be significantly suppressed. Because the surface states are topologically protected, the surface states can still carry the supercurrent in the hole conduction region, which may be responsible for the saturated I_c as V_g up to −20 V.

When irradiated with $f = 6.7$ GHz microwave, the Shapiro steps are observed at integer voltages $V_n = nhf/2e$, starting from $n = 0, 1, \ldots$, as shown in Fig. 2(a). The $n = 1$ step is nearly missing at 9 dBm [Fig. 2(a)], which is due to the system entering into the oscillatory regime [6]. Under a low frequency of 2 GHz, the $n = 1$ step is missing at a lower power of −10.25 and −5 dBm, as shown in Fig. 2(b). With only several I-V curves under rf irradiation, we cannot use the missing of the $n = 1$ step as evidence for the 4π-periodic supercurrent.

To further study the 4π-periodic supercurrent in our devices, we derive the evolution of step size for constant voltages $V_n = nhf/2e$ utilizing the binning method [6]. Figures 3(a), 3(b) show the 2D map of differential resistance dV/dI as a function of dc current bias I_{dc} and rf power, taken at 6.7 and 2 GHz, respectively. For $f = 6.7$ GHz, Shapiro steps emerge one by one. As rf power is increased, all steps gradually demonstrate oscillatory patterns. While for $f = 2$ GHz, the evolution of Shapiro steps seems more complicated, which is different from the conventional pattern of high frequency (6.7 GHz). To distinguish the different steps, the rf power dependence of step size from $n = 0$ to 4 is plotted in Figs. 3(c), 3(d). The Shapiro step size versus rf power indeed obeys the quasi-Bessel function [39] for high frequency $f =$ 6.7 GHz, as illustrated in Fig. 3(c). For $f = 2$ GHz, the maximum amplitude of the $n = 1$ step is clearly suppressed contrary to the neighboring $n = 2$ step in the low power regime [Fig. 3(d)], which may result from the 4π-periodic supercurrent contribution [6]. To describe the suppression of the $n = 1$ step, we introduce an indicator $Q_{12} = w_1/w_2$, where w_1 (w_2) denotes the maximum amplitude of the first lobe of $n = 1$ ($n = 2$) step [6], as indicated by arrows in Fig. 3(c). As discussed by Dominguez *et al.* [40], the contribution of the 4π-periodic supercurrent would be visible when the frequency is lower than the characteristic

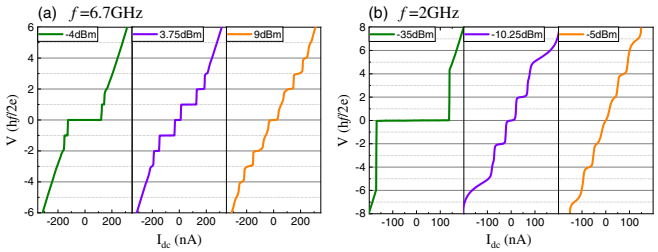

FIG. 2. Response to rf radiation for $V_g = 0$ V. (a) I-V curves for different rf powers at frequency $f = 6.7$ GHz. The voltage scale is in normalized units $hf/2e$ to emphasize the presence of Shapiro steps. (b) I-V curves for different rf powers at $f = 2$ GHz.

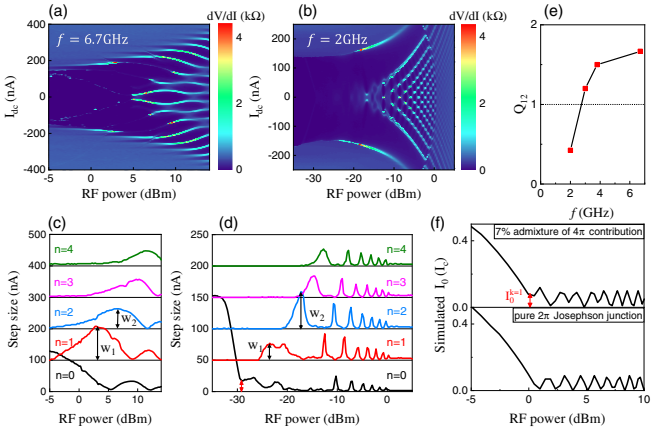

FIG. 3. Shapiro steps versus rf power. (a)–(b) Map of differential resistance dV/dI as a function of dc current bias $I_{\rm dc}$ and rf power, for frequencies $f = 6.7$ and 2 GHz, respectively. (c)–(d) rf power dependence of step size for different integer index, from $n = 0$ to 4, extracted from (a)–(b). For clarity, different curves in (c) and (d) are shifted vertically. Here the step size I_0 is defined as the half width of $n = 0$ Shapiro plateau. (e) The ratio, Q_{12}, between the $n = 1$ and 2 steps, as a function of frequency f. The dashed line indicates the theoretical value of Q_{12} for a conventional 2π junction (close to unity). (f) Simulated Shapiro response of $n = 0$ step under low irradiation frequency (here $f = 0.1f_c$, $f_c = 2eI_cR_n/h$). The below corresponds to a pure 2π Josephson junction, while the top is for a junction with 7% admixture of 4π-periodic contribution, in which residual supercurrent of first node emerges, noted $I_0^{k=1}$ (see the red arrow).

frequency $f_{4\pi} = 2eI_{4\pi}R_n/h$ (R_n is the normal state resistance). $f_{4\pi}$ is estimated around 3.3 GHz, assuming $I_{4\pi} \sim 0.1I_{2\pi}(I_{2\pi} \simeq I_c)$ in our junction. In Fig. 3(e), we plot the ratio Q_{12} as a function of irradiation frequency f. Just as calculated, the experimental Q_{12} tends to a low value when $f \lesssim 3.3$ GHz, in which the 4π-periodic supercurrent gradually dominates the rf response. Furthermore, we observe the obvious residual supercurrent [36] at $n = 0$ Shapiro step in low frequency of 2 GHz [indicated by the red arrow in Fig. 3(d)], which provides a direct and distinct signature of 4π-periodic contribution.

For clarity, we introduce the resistively shunted junction (RSJ) model [39] to simulate the $n = 0$ Shapiro response, that is, the time-averaged voltage response to the rf signals in our current bias experiment. The I-V curves can be numerically obtained by solving the equation: $i_{\rm dc} + i_{\rm rf}\sin(\Omega\tau) = i_c^{2\pi}\sin\phi + i_c^{4\pi}\sin(\phi/2) + d\phi/d\tau$, where ϕ is the superconducting phase difference, $\tau = tI_cR_n2e/\hbar$, $i = I/I_c$,$\Omega = f/f_c$ with $f_c = I_cR_n2e/h$, and $i_c^{2\pi}$ and $i_c^{4\pi}$ are the 2π- and 4π- periodic current ratios, respectively [39–40]. Considering the parameter values in our Cd_3As_2 nanowire-based Josephson junction, the Ω is $\sim$0.1 for $V_g = 0$ V, when irradiated with $f = 2$ GHz microwave. As shown in Fig. 3(f), with only 7% admixture of 4π-periodic contribution ($\Omega = 0.1$), the junction still displays obvious residual supercurrent at the $n = 0$ step, where the simulated step size I_0 is also defined as the half width of the whole $n = 0$ Shapiro plateau. Similarly, we found that a recent work [36] also reports the residual supercurrent in the topological insulator Bi_2Se_3-based Josephson junction, providing a compelling signature of 4π-periodic contribution.

Because of the large surface-to-volume ratio, the contribution of surface state transport is significant and A-B oscillations are commonly observed in Cd_3As_2 nanowires [21,22]. As mentioned before, the 4π-periodic supercurrent is closely linked with surface gapless Andreev bound states. But due to residual bulk transport, the 4π-periodic supercurrent is usually accompanied by conventional 2π-periodic modes, which make the analysis of 4π-periodic supercurrent more complicated. To enhance surface states contribution and increase the proportion of 4π-periodic supercurrent, we study the evolution of Shapiro steps under gate modulation. The Dirac point of this device is at about -6 V [Fig. 1(b)]. At $V_g = 10$ V, the Fermi level is in the conduction band, and the ratio of surface state to bulk state transport would be decreased, resulting in no suppression of $n = 1$ step at $f = 2$ GHz, as shown in Figs. 4(a), 4(c).

But at $V_g = -30$ V, the disappearance of $n = 1$ step is clearly observed at $f = 0.69$ GHz, as shown in Fig. 4(b). For the Fermi level in the valance band, the bulk related transport is restrained due to low mobility of holes, while the surface state transport is amplified in view of its high mobility, benefiting from the topologically protected Fermi

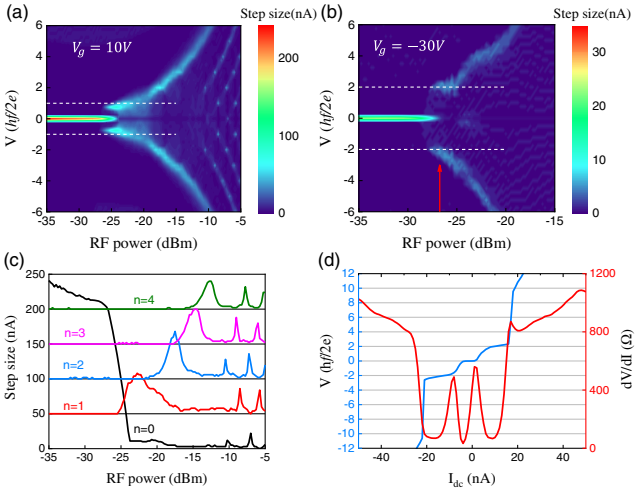

FIG. 4. rf response modulated by gate voltage. (a)–(b) Color map of step size as a function of normalized voltage V and rf power, for $V_g = 10$ V ($f = 2$ GHz) and $V_g = -30$ V ($f = 0.69$ GHz), respectively. The red arrow in (b) indicates the line cut used to plot in (d). Dashed lines are guides to the eyes. (c) rf power dependence of step size for different integer index, from $n = 0$ to 4, extracted from (a). For clarity, different curves are shifted vertically. (d) The normalized voltage V and differential resistance dV/dI versus current bias $I_{\rm dc}$ for $V_g = -30$ V, under rf power $= -26.75$ dBm [indicated by red arrow in (b)].

arcs [21,22,38]. Therefore, the significant contribution of surface state transport produces the notable 4π-periodic supercurrent, resulting in the missing of the $n = 1$ step. From Fig. 4(d), we can clearly judge the appearance of the $n = 2$ Shapiro step in the beginning of low power (instead of the $n = 1$ step). Higher indices of Shapiro steps are not clearly observed here, which may result from weak coupling between the device and rf irradiation. Absent in the traditional 2π-periodic mode, the missing of the $n = 1$ step reveals the significant contribution of the 4π-periodic supercurrent.

To conclude, we have systematically studied the rf response of Cd_3As_2 nanowire-based Josephson junctions. Under low frequency irradiation, suppression of the $n = 1$ step and residual supercurrent at the $n = 0$ step are observed in the low power regime, together suggesting the contribution of the 4π-periodic supercurrent. By tuning the gate voltage to enhance the surface state contribution, the odd ($n = 1$) Shapiro step is further suppressed. The results of the 4π-periodic supercurrent from surface states in the Cd_3As_2 nanowire-based Josephson junction help to explore topological superconductivity in Dirac semimetals.

This work was supported by National Key Research and Development Program of China (No. 2016YFA0300802), and National Natural Science Foundation of China (No. 61825401 and No. 11774004). C. L. and A. B. acknowledge the financial support by the Netherlands Organization for Scientific Research (NWO) through a VENI grant, the European Research Council (ERC) through a Consolidator Grant, and the COST project "Nanoscale coherent hybrid devices for superconducting quantum technologies"—Action CA16218.

*These authors contributed equally to this work.
†liaozm@pku.edu.cn
‡a.brinkman@utwente.nl

[1] L. Fu and C. L. Kane, Phys. Rev. Lett. **100**, 096407 (2008).
[2] M. Veldhorst, M. Snelder, M. Hoek, T. Gang, V. K. Guduru, X. L. Wang, U. Zeitler, W. G. van der Wiel, A. A. Golubov, H. Hilgenkamp, and A. Brinkman, Nat. Mater. **11**, 417 (2012).
[3] S. Cho, B. Dellabetta, A. Yang, J. Schneeloch, Z. Xu, T. Valla, G. Gu, M. J. Gilbert, and N. Mason, Nat. Commun. **4**, 1689 (2013).
[4] M. X. Wang, C. H. Liu, J. P. Xu, F. Yang, L. Miao, M. Y. Yao, C. L. Gao, C. Y. Shen, X. C. Ma, X. Chen, Z. A. Xu, Y. Liu, S. C. Zhang, D. Qian, J. F. Jia, and Q. K. Xue, Science **336**, 52 (2012).
[5] H. H. Sun, K. W. Zhang, L. H. Hu, C. Li, G. Y. Wang, H. Y. Ma, Z. A. Xu, C. L. Gao, D. D. Guan, Y. Y. Li, C. Liu, D. Qian, Y. Zhou, L. Fu, S. C. Li, F. C. Zhang, and J. F. Jia, Phys. Rev. Lett. **116**, 257003 (2016).
[6] J. Wiedenmann, E. Bocquillon, R. S. Deacon, S. Hartinger, O. Herrmann, T. M. Klapwijk, L. Maier, C. Ames, C. Brune, C. Gould, A. Oiwa, K. Ishibashi, S. Tarucha, H. Buhmann, and L. W. Molenkamp, Nat. Commun. **7**, 10303 (2016).
[7] E. Bocquillon, R. S. Deacon, J. Wiedenmann, P. Leubner, T. M. Klapwijk, C. Brune, K. Ishibashi, H. Buhmann, and L. W. Molenkamp, Nat. Nanotechnol. **12**, 137 (2017).
[8] X. G. Wan, A. M. Turner, A. Vishwanath, and S. Y. Savrasov, Phys. Rev. B **83**, 205101 (2011).
[9] Z. J. Wang, H. M. Weng, Q. S. Wu, X. Dai, and Z. Fang, Phys. Rev. B **88**, 125427 (2013).
[10] S. Y. Xu, C. Liu, S. K. Kushwaha, R. Sankar, J. W. Krizan, I. Belopolski, M. Neupane, G. Bian, N. Alidoust, T. R. Chang, H. T. Jeng, C. Y. Huang, W. F. Tsai, H. Lin, P. P. Shibayev, F. C. Chou, R. J. Cava, and M. Z. Hasan, Science **347**, 294 (2015).
[11] B. Q. Lv, H. M. Weng, B. B. Fu, X. P. Wang, H. Miao, J. Ma, P. Richard, X. C. Huang, L. X. Zhao, G. F. Chen, Z. Fang, X. Dai, T. Qian, and H. Ding, Phys. Rev. X **5**, 031013 (2015).
[12] S. Kobayashi and M. Sato, Phys. Rev. Lett. **115**, 187001 (2015).
[13] T. Hashimoto, S. Kobayashi, Y. Tanaka, and M. Sato, Phys. Rev. B **94**, 014510 (2016).
[14] S. Wang, B.-C. Lin, A.-Q. Wang, D.-P. Yu, and Z.-M. Liao, Adv. Phys. X **2**, 518 (2017).
[15] M. D. Bachmann, N. Nair, F. Flicker, R. Ilan, T. Meng, N. J. Ghimire, E. D. Bauer, F. Ronning, J. G. Analytis, and P. J. W. Moll, Sci. Adv. **3**, e1602983 (2017).
[16] Z. K. Liu, J. Jiang, B. Zhou, Z. J. Wang, Y. Zhang, H. M. Weng, D. Prabhakaran, S. K. Mo, H. Peng, P. Dudin, T. Kim, M. Hoesch, Z. Fang, X. Dai, Z. X. Shen, D. L. Feng, Z. Hussain, and Y. L. Chen, Nat. Mater. **13**, 677 (2014).
[17] M. Neupane, S. Y. Xu, R. Sankar, N. Alidoust, G. Bian, C. Liu, I. Belopolski, T. R. Chang, H. T. Jeng, H. Lin, A. Bansil, F. Chou, and M. Z. Hasan, Nat. Commun. **5**, 3786 (2014).
[18] S. Jeon, B. B. Zhou, A. Gyenis, B. E. Feldman, I. Kimchi, A. C. Potter, Q. D. Gibson, R. J. Cava, A. Vishwanath, and A. Yazdani, Nat. Mater. **13**, 851 (2014).
[19] T. Liang, Q. Gibson, M. N. Ali, M. Liu, R. J. Cava, and N. P. Ong, Nat. Mater. **14**, 280 (2015).
[20] C. Z. Li, L. X. Wang, H. Liu, J. Wang, Z. M. Liao, and D. P. Yu, Nat. Commun. **6**, 10137 (2015).
[21] L. X. Wang, C. Z. Li, D. P. Yu, and Z. M. Liao, Nat. Commun. **7**, 10769 (2016).
[22] B. C. Lin, S. Wang, L. X. Wang, C. Z. Li, J. G. Li, D. P. Yu, and Z. M. Liao, Phys. Rev. B **95**, 235436 (2017).
[23] A. C. Potter, I. Kimchi, and A. Vishwanath, Nat. Commun. **5**, 5161 (2014).
[24] P. J. Moll, N. L. Nair, T. Helm, A. C. Potter, I. Kimchi, A. Vishwanath, and J. G. Analytis, Nature (London) **535**, 266 (2016).
[25] L. Aggarwal, A. Gaurav, G. S. Thakur, Z. Haque, A. K. Ganguli, and G. Sheet, Nat. Mater. **15**, 32 (2016).
[26] H. Wang, H. Wang, H. Liu, H. Lu, W. Yang, S. Jia, X. J. Liu, X. C. Xie, J. Wei, and J. Wang, Nat. Mater. **15**, 38 (2016).
[27] L. P. He, Y. T. Jia, S. J. Zhang, X. C. Hong, C. Q. Jin, and S. Y. Li, npj Quantum Mater. **1**, 16014 (2016).
[28] L. Fu and C. L. Kane, Phys. Rev. B **79**, 161408 (2009).
[29] L. Jiang, D. Pekker, J. Alicea, G. Refael, Y. Oreg, and F. von Oppen, Phys. Rev. Lett. **107**, 236401 (2011).

[30] D. M. Badiane, M. Houzet, and J. S. Meyer, Phys. Rev. Lett. **107**, 177002 (2011).
[31] F. Zhang and C. L. Kane, Phys. Rev. B **90**, 020501 (2014).
[32] C. Li, J. C. de Boer, B. de Ronde, S. V. Ramankutty, E. van Heumen, Y. Huang, A. de Visser, A. A. Golubov, M. S. Golden, and A. Brinkman, Nat. Mater. **17**, 875 (2018).
[33] H. J. Kwon, K. Sengupta, and V. M. Yakovenko, Eur. Phys. J. B **37**, 349 (2003).
[34] P. San-Jose, E. Prada, and R. Aguado, Phys. Rev. Lett. **108**, 257001 (2012).
[35] H. Courtois, M. Meschke, J. T. Peltonen, and J. P. Pekola, Phys. Rev. Lett. **101**, 067002 (2008).
[36] K. Le Calvez, L. Veyrat, F. Gay, P. Plaindoux, C. Winkelmann, H. Courtois, and B. Sacépé, arXiv:1803.07674.
[37] W. Yu, W. Pan, D. L. Medlin, M. A. Rodriguez, S. R. Lee, Z.-q. Bao, and F. Zhang, Phys. Rev. Lett. **120**, 177704 (2018).
[38] C.-Z. Li, C. Li, L.-X. Wang, S. Wang, Z.-M. Liao, A. Brinkman, and D.-P. Yu, Phys. Rev. B **97**, 115446 (2018).
[39] P. Russer, J. Appl. Phys. **43**, 2008 (1972).
[40] F. Domínguez, F. Hassler, and G. Platero, Phys. Rev. B **86**, 140503(R) (2012).